DALTON
FULL PAPER

A novel ruthenium surfactant: electronic spectra, ZINDO analysis and Langmuir–Blodgett studies of *trans*-dichloro(6,6′-bis(*N*-dodecylbenzimidazol-2-yl)-2,2′-bipyridine)ruthenium(II) †

Matthew F. Ryan,[a] Robert A. Metcalfe,[b] A. B. P. Lever[b] and Masa-aki Haga*[c]

[a] *Department of Chemistry and Physics, Purdue University Calumet, Hammond, Indiana, 46323, USA*
[b] *Department of Chemistry, 4700 Keele Street, York University, Toronto, Ontario, Canada M3J 1P3*
[c] *Department of Applied Chemistry, Chuo University, 1-13-27 Kasuga, Bunkyo-ku, Tokyo 112-8551, Japan*

Received 16th March 2000, Accepted 19th May 2000
Published on the Web 30th June 2000

The complex, dichloro(6,6′-bis(*N*-dodecylbenzimidazol-2-yl)-2,2′-bipyridine)ruthenium(II), Ru(ddbbbpy)Cl_2 was prepared from the reaction of the free ligand and $RuCl_2(Me_2SO)_4$. Structural characterization of the compound by ^{1}H NMR revealed that 6,6′-bis(*N*-dodecylbenzimidazol-2-yl)-2,2′-bipyridine ligand lies symmetrically about the equatorial plane with the chlorides axial to each other. The electronic structure of the compound shows several ligand π–π* transitions in the ultraviolet and a broad d_π–p_{π^*} MLCT manifold in the visible region of the spectrum. A ZINDO/S calculation reproduces, in some detail, the general features of the electronic spectrum of the title species. The electronic characteristics of the frontier orbitals are analysed. The parent neutral compound shows a fully reversible oxidation wave at −0.04 V *vs*. the Cp_2Fe^+/Cp_2Fe couple in 0.1 M $(C_4H_9)_4NPF_6/CH_2Cl_2$. The low temperature (77 K) EPR spectrum of the one-electron oxidized product is typical for a rhombohedrally distorted Ru(III) complex with *g* values of 2.73, 2.20 and 1.82. Surface analysis of the parent complex as studied using Langmuir–Blodgett methods show a typical isotherm from which an area per molecule of 126 Å^2 can be derived. Thin films of the complex were readily transferred to quartz and indium doped tin oxide (ITO) plates. Thin films are conductive as indicated by the cyclic voltammetry of the complexes on ITO slides.

Introduction

Applications of transition-metal complexes as molecular electronic devices are often dependent on compounds that have specific properties and electronic characteristics. Ruthenium–bipyridine systems $[Ru(bpy)_3]^{q+}$ and $[Ru(bpy)_2L_2]^{q+}$, where L denotes auxiliary ligation, used as the building blocks in the fabrication of molecular assemblies have been an important focus of such research because ruthenium complexes may serve as redox-active and photo-induced sensitizers.[1–4]

Metal complexes formed as thin solid films are particularly useful for designing potential devices because the two-dimensional ordering of their films can be readily controlled.[5,6] Accordingly, Langmuir–Blodgett (LB) techniques have become an invaluable tool for the construction of molecular assemblies. For example, numerous LB strategies have been used to construct thin films, with tunable electrochemical and photophysical properties, based on the well-characterized photosensitizer $[Ru(bpy)_3]^{2+}$. Some strategies include incorporating ruthenium compounds in hydrophobic LB films[7,8] or designing $[Ru(bpy)_3]^{2+}$ derivatives with hydrophobic functions to help stabilize monolayer formation.[9–11] De Armond incorporated $[Ru(bpy)_3]^{2+}$ from an aqueous subphase into stearic acid films by cationic exchange.[8b] Bard has directly formed hydrophobic LB films from amphiphilic $[Ru(bpy)_3]^{2+}$ derivatives and his group was first to demonstrate electrogenerated chemiluminescence from a Langmuir monolayer.[9] Matsuda and co-workers have examined in detail the electrode kinetics of polypyridine ruthenium and osmium surfactants formed as monolayer films on tin oxide electrodes by LB techniques.[10] The optical properties of monolayer assemblies based on $[Ru(bpy)_3]^{2+}$ have also been explored.[11] De Armond and co-workers have also examined LB films of tris(phenylpyridine)iridium(III)[12] and the square-planar system bis(2-(2-thienyl)pyridine)platinum(II) mixed with stearic acid.[13]

For the most part, the ruthenium–bipyridine complexes have an octahedral *cis* configuration.[1,2] By comparison, fewer studies of *trans* ruthenium–bipyridine complexes have been reported.[14–16]

Interest in ruthenium imidazole complexes has grown as scientists search for novel systems that may potentially serve as molecular electronic devices.[17–19] Imidazole derivatives are important building blocks in the synthesis of large molecular assemblies because they can serve as bridges between the redox centers of polynuclear metal complexes. An imidazole can coordinate to a metal ion as either the neutral (HIm) or deprotonated form (Im), thus most studies involving ruthenium–bipyridine systems with imidazole have focused on the electrochemical and spectroscopic properties in relation to acid–base chemistry.[17]

To explore the coordination chemistry of ruthenium imidazole systems but without the complications of deprotonation from the N–H imino group, *N*-alkyl derivatives can be studied. Accordingly, we have investigated the chemistry of a novel ruthenium complex containing the tetradentate ligand 2,2′,6,6′-bis(*N*-dodecylbenzimidazol-2-yl)-2,2′-bipyridine) (Scheme 1).

† Electronic supplementary information (ESI) available: NMR data, spectroelectrochemical oxidation of the parent species, colour pictures of the frontier molecular orbitals, the *x*, *y*, *z* coordinate frame of reference for the ZINDO calculation and a CHIME readable display of the parent molecule. See http://www.rsc.org/suppdata/dt/b0/b002123g/

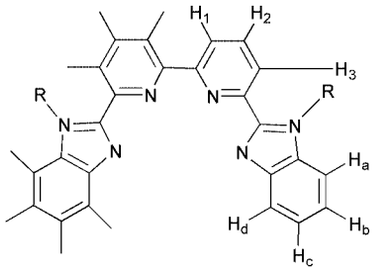

Ligand	R
H_2bbbpy	H
dmbbbpy	CH_3
ddbbbpy	$C_{12}H_{25}$

Scheme 1

We have already reported our preliminary LB analysis,[18] and we now provide a more complete account of the solution and surface chemistry of the title complex in addition to computational analysis. The INDO model, as developed by Zerner[20–28] in the ZINDO program has been shown to be very useful in reproducing the electronic spectra and the structure of ruthenium(II) complexes.[29–34] It is used here to understand the electronic structure of the title complex.

Results and discussion

Synthetic studies

The reaction of $RuCl_2(Me_2SO)_4$ with the free ligand in either toluene or methylene chloride was used to prepare Ru(ddbbbpy)Cl_2 as a dark purple powder in good yield. Alternatively, $[RuCl_2(cym)_2]_2$ (cym = *p*-cymene) has been used to prepare Ru(H_2bbbpy)Cl_2 and Ru(dmbbbpy)Cl_2[18,19] (where H_2bbbpy and dmbbbpy are the corresponding ligands where the dodecyl group is replaced by hydrogen or methyl respectively). Elution (methylene chloride/hexane) of Ru(ddbbbpy)Cl_2 over silica gel yielded only one fraction and elemental analysis confirms the purity of the complex as a monohydrate.[18] The electronic absorption spectrum of Ru(ddbbbpy)Cl_2 in methanol at 25 °C shows no change upon addition of acid indicating that the four sp^2-nitrogen atoms are coordinated to the ruthenium center. The title complex is more soluble (*ca.* 0.1 g/mL^{-1}) in weakly polar solvents such as methylene chloride, chloroform, and toluene than are Ru(H_2bbbpy)Cl_2 and Ru(dmbbbpy)Cl_2; the relative variations in solubility are attributed to the long alkyl chains of Ru(ddbbbpy)Cl_2.

Only a slight excess of ligand (≈1.2 equivalents) is needed to prepare Ru(ddbbbpy)Cl_2 presumably due to a strong chelate effect as manifested by the ability of the ligand to displace all four Me_2SO ligands of the starting Ru complex. For example, bipyridine and phenanthroline react with $RuCl_2(Me_2SO)_4$ to displace only two Me_2SO molecules forming $RuCl_2(Me_2SO)_2$L. Displacement of four Me_2SO ligands was only observed by refluxing $RuCl_2(Me_2SO)_4$ in neat ligand as is the case for the formation of $RuCl_2(py)_4$.[35] Preparations that used a 10-fold excess of ligand gave only slight increases in the overall yield.

^{1}H NMR

The ^{1}H NMR of Ru(ddbbbpy)Cl_2 recorded in $(CD_3)_2SO$ consists of five sets of resonances in the aromatic region. Proton are assigned as H_1, H_a/H_3, H_d, H_2 and H_b/H_c in order of low-field to high magnetic field, consistent with C_2-symmetry for the compound. These assignments are based upon decoupling experiments reported for Ru(dmbbbpy)Cl_2.[19] These assignments are also consistent with the proton spectrum of the free ligand[19] and Ru(bpy)$_2Cl_2$.[17,36] Signals for H_3 and H_a overlap a large doublet and the shifts H_b and H_c appear as a multiplet. The bipyridyl protons appear as a doublet (H_1), doublet (H_3), and triplet (H_2) in increasing field strength. The change in the chemical resonances of the imidazole protons relative to the free ligand indicate strong σ-donation of the nitrogen lone-pairs to Ru(II).[19]

A molecular model of Ru(ddbbbpy)Cl_2 indicates that the chelate must distort from planarity and thus lower its symmetry in order to coordinate to the metal center. The resulting increase in van der Waals forces between the adjacent H_1 protons will lead to their downfield shift.[36] A planar ligand arrangement around the Ru(II) center will also shift the H_2 protons due to Ru(II) π-backbonding to the pyridine ring.[19] Distortions of the ligand from planarity however should relieve steric repulsions of the benzimidazole rings and help attenuate the through-space proton–proton interactions. For example, in the absence of any strain-relieving distortion, the H_d protons would be deshielded to an even greater extent.[17g]

Computational studies

The title complex, but with replacement of the long chains by a methyl group, was geometry optimized using the ZINDO/1 method (see Experimental section).[20–28] The Ru–N(bpy) optimized at 200 pm which is rather shorter than found with simple bipyridine ruthenium(II) species, while the Ru–N(imidazole) fragment bonds were slightly longer (206 pm) than the former distances. The Ru–Cl bond lengths were 237 pm and the Cl–Ru–Cl angle is very close to 180°. The optimized xyz file can be observed, using CHIME, as supporting information.

The overall symmetry of both complex and free ligand approximates to C_{2v} with the C_2 axis bisecting the bipyridine NN coordinating fragment. The deviation from C_{2v} symmetry is due to the buckling of the benzimidazole residues to minimize steric hindrance. The actual symmetry is C_2. The C_2 axis is defined as *z* and the approximate plane of the molecule is *xz*. Table 1 shows the molecular orbital energies of the frontier orbitals of the complex together with a breakdown of the squared coefficients into ruthenium, bipyridine and benzimidazole localized. Although the ligand is a single entity, some insight into the structure can be obtained by factoring it into its bipyridine and benzimidazole components. Frontier molecular orbitals of the complex are shown in Fig. 1.

The molecular orbitals of the free ligand (Fig. 2) were derived by removing the ruthenium and chlorine atoms (from the computer file) and recalculating the MOs of the ligand but without re-optimizing the geometry.

Approximating the symmetry to C_{2v}, the three d (t_{2g}) orbitals can be seen fairly closely to have #88 (HOMO) δ (*xy*, a) symmetry, degenerate with #87 (HOMO) π (*yz*, b) symmetry, and #86 (HOMO − 2) σ (z^2, a) symmetry, with respect to the bipyridine NN fragment, where the a,b refer to symmetry in the group C_2. The degeneracy of #87 and #88 is interesting since there is no requirement for degeneracy in the point group C_2. If it is not accidental, then the molecule is behaving as if there is an effective c_4 axis perpendicular to the molecular plane. Indeed, a *cis*-square system, MX_2Y_2 although of C_{2v} symmetry, does behave[37] as though it has such a c_4 axis with energy levels appropriate for the point group D_{4h}. The reason for this is that the effective field along the *x* and *y* axes is the same, being the sum of the *X* and *Y* ligand contributions, and hence there is a virtual c_4 axis. This is apparently the case here.

Orbital #86 (HOMO − 2, a) is fairly pure Ru since, lying in the plane of the ligand, it interacts only weakly therewith. There are three fairly low lying empty π* orbitals. Orbitals #90 (LUMO + 1, b) is mostly localized on the bipyridine fragment, while orbitals #89 (LUMO, b) and #91 (LUMO + 2, a) are distributed more evenly over the whole molecule.

The free ligand HOMO-1 (#76), LUMO (#78) and LUMO + 2 (#80) have "b" symmetry and may then interact with the metal *yz* (b) d_π-orbital while the HOMO (#77) and

Table 1 Molecular orbital energies of the title complex and contributions of atomic orbitals of ruthenium, chloride, bipyridine and benzimidazole fragments

Orbital[a]	Energy/eV	%Ru	%Cl	%Benzimidazole	%bpy	Symmetry[b]
98	1.239	1	0	72	27	b
97	1.088	65	26	3	5	a,σ
96	0.938	0	0	78	21	a
95	0.862	0	0	97	3	b
94	0.809	0	0	85	15	a
93	0.621	0	0	67	33	b
92	0.202	0	0	25	75	a
91	−0.772	11	0	40	49	a, *xy*, δ
90	−0.896	6	0	5	89	b, *yz*, π
89L	−1.198	4	2	43	52	b, *yz*, π
88H	−6.512	62	5	16	17	e(a), *xy*, δ
87H	−6.512	63	6	13	18	e(b), *yz*, π
86	−6.700	87	1	7	5	a, $z^2 + x^2 - y^2$, σ
85	−8.059	2	3	77	18	a, *xy*, δ
84	−8.223	4	7	81	8	b, *yz*, π
83	−8.373	1	18	78	2	b, *yz*, y, π
82	−8.527	3	11	86	1	a, *xy*, δ
81	−8.968	4	66	19	11	b, *y*, π
80	−9.162	0	34	18	48	a
79	−9.243	0	95	3	2	b
78	−9.288	1	94	2	3	a

[a] H = HOMO which is doubly degenerate. L = LUMO. [b] *xy*, *yz*, z^2 and $x^2 - y^2$ are d orbitals, *y* is the p_y orbital.

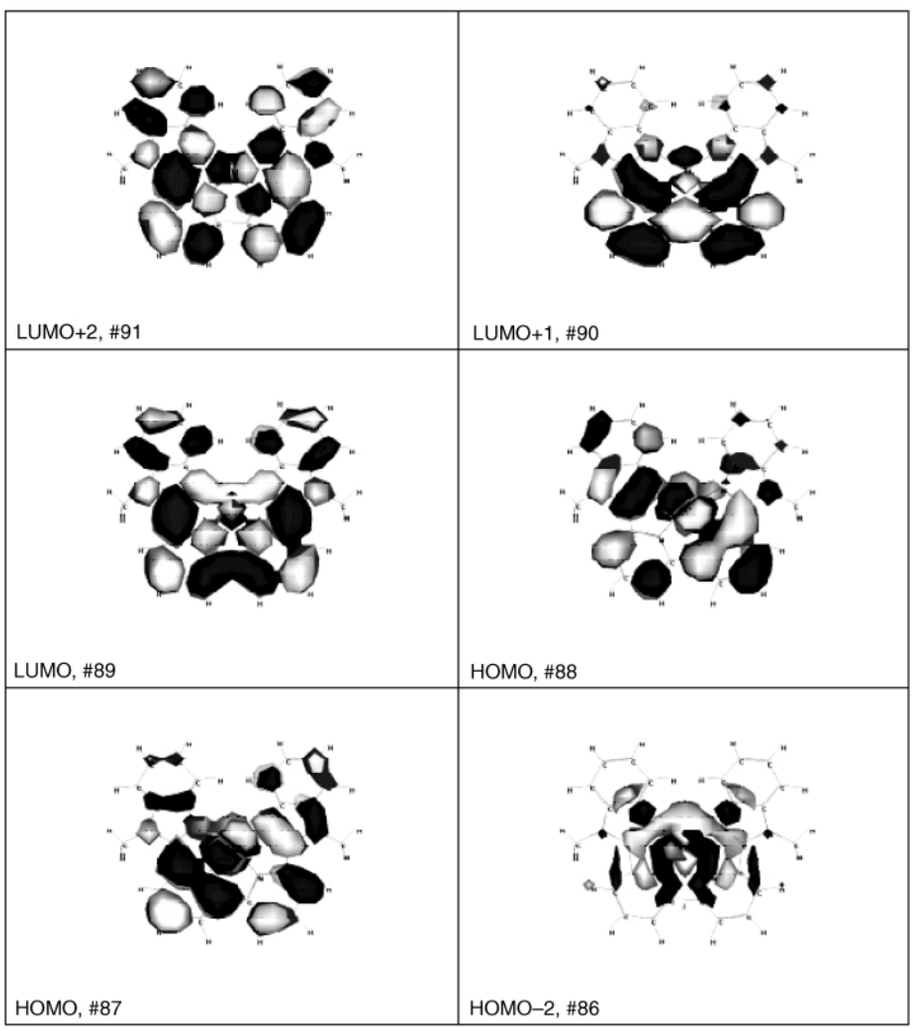

Fig. 1 Sketch of some frontier molecular orbitals for the parent complex. See supporting information for sketches of other frontier orbitals of the complex and the free ligand (in colour).

LUMO + 1 (#79) have "a" symmetry appropriate to interact with *xy* (a), the d_δ orbital.

In the complex, back donation into the bipyridine fragment occurs in the #90 (LUMO + 1) orbital *via* the π-interaction of d_π, *yz* with the free ligand LUMO #78, and to a degree typical of simple ruthenium bipyridine species.[34] Orbital #89 (LUMO) arises from coupling of d_π with the free ligand LUMO + 2 (#80).

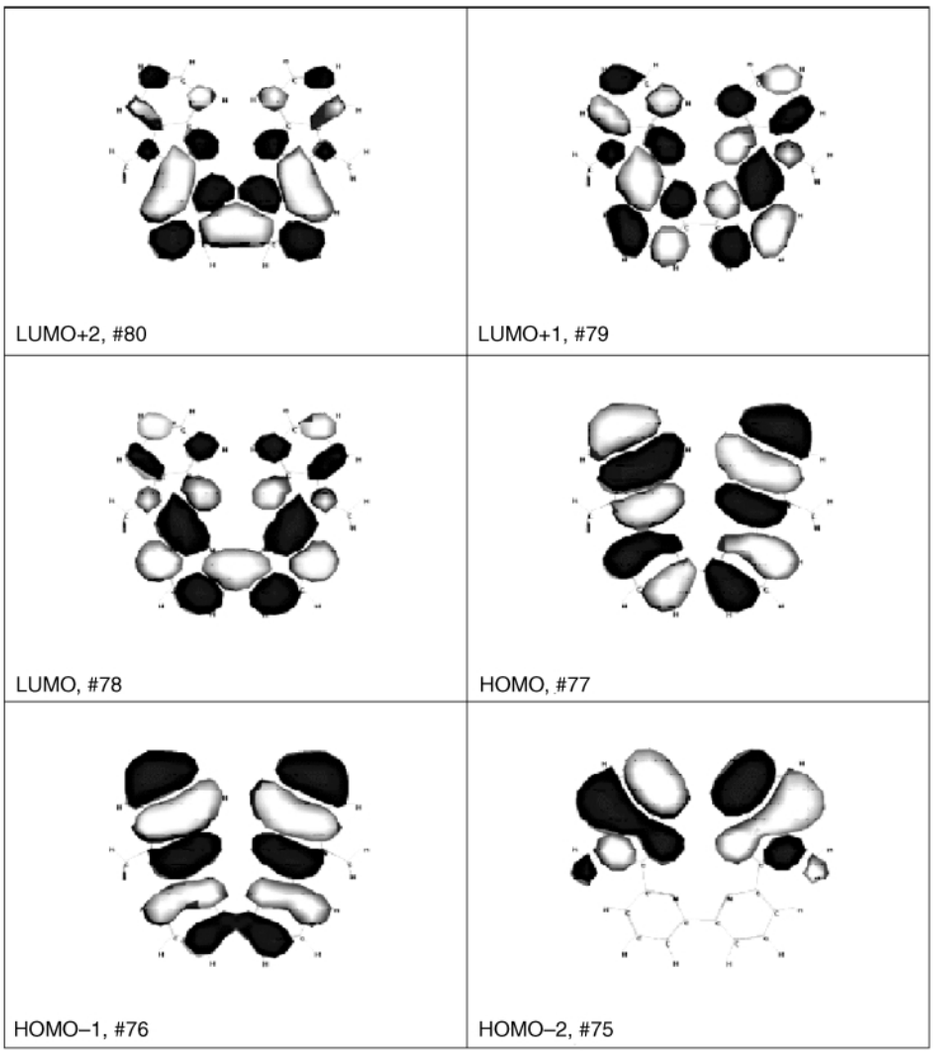

Fig. 2 Sketch of some frontier molecular orbitals for the free ligand in the conformation of the complex. See supporting information for sketches of other frontier orbitals of the complex and the free ligand (in colour).

Back donation into the LUMO + 2 (#91) is surprisingly large (*ca.* 11%, Table 1) and involves the d_δ-orbital coupled to free ligand LUMO + 1 (#79). The reason for the enhanced degree of back donation can be seen in the representation of this molecular orbital (#91) in Fig. 1. It is evident that the d_δ orbital is well placed to back donate into π* orbitals of both the bipyridine and benzimidazole fragments at the same time. A unique observation.

Absorption spectra

The electronic spectrum (Table 2, Fig. 3) of Ru(ddbbbpy)Cl_2 shows a broad absorption manifold in the visible region (13000–25000 cm^{-1}) which is a series of overlapping $d_\pi \rightarrow p_{\pi^*}$ MLCT bands.[18,19] Two narrow absorption peaks at 27200–28400 cm^{-1} are also MLCT in origin. In addition there are two strong ligand based π–π* transitions in the ultraviolet region, to 42000 cm^{-1}, corresponding to similar absorption to the free ligand being relatively unshifted upon coordination.[19]

The existence of three low lying π* orbitals explains the presence of so many spectrum overlapping Ru d→π* MLCT transitions. A gaussian deconvolution revealing at least six absorption bands is shown in Fig. 3 (inset). The ZINDO/S calculation[20–28] reproduces these general features and predicts as many as 12 MLCT transitions of reasonable intensity ($f \geq 0.01$) up to 31000 cm^{-1} (Table 2). These arise, in this rather low symmetry molecule from transitions from each of the $d(t_{2g})$ orbitals to the aforementioned three low lying π* orbitals localized on the ddbbpy ligand but having a significant metal contribution. Additional MLCT bands (Table 2) lie above 25000 cm^{-1} and will overlap the lower lying π–π* transitions. We have assigned the specific experimental transitions, in terms of their general agreement in energy and relative intensities to the predicted data. The vertical bars in Fig. 3 illustrate the positions of the predicted transitions and are scaled to the maximum visible region intensity (see Experimental section). There is really quite good agreement between predicted and experimental data in terms of both energy and relative intensity.

Electrochemistry

The cyclic voltammetry of Ru(ddbbbpy)Cl_2 was investigated at ambient temperature in CH_2Cl_2 with 0.1 M $(C_4H_9)_4NPF_6$ as supporting electrolyte. The oxidation potential of Ru^{II}(ddbbbpy)Cl_2 is $E_{\frac{1}{2}} = -0.04$ V *vs.* Fc^+/Fc (+0.63 V *versus* NHE); the redox wave exhibits $I_{pa}/I_{pc} = 1$ and $E_{pp} = 80$ mV which is consistent with a reversible one-electron oxidation process. The wave is stable with respect to continued cycling. A linear relationship between anodic peak current and square root potential scan rate is observed below 200 mV s^{-1}. The reduction wave at −1.66 V *vs.* Fc^+/Fc is irreversible[19] however upon repeated cycling the return (anodic) wave stabilizes with E_{pp} = 140 mV at a scan rate of 100 mV s^{-1}.

Spectroelectrochemistry and electron paramagnetic resonance spectra

The reversibility of the controlled potential oxidation clearly demonstrates that no irreversible structural changes occur

Table 2 Comparison of experimental and predicted transition energies (cm^{-1}), with assignments

Experimental[a]	Predicted[b]	Assignment[c]
14690 (7.3, 2619)	13300 (0.04)	86, 88→89
17050 (8.2, 2370)	16650 (0.04)	87→91
	17900 (0.03)	88→91; 87, 89→90 (vm)
21335 (4.7, 1824)	19150 (0.05)	86, 88→89; 86, 88→90 (vm)
	19900 (0.15)	86, 88→90; 88→89
27200 (24.8)	24900 (0.12)	87→90, 88→91
28400 (26.9)	28450 (0.33)	87→92; 85→89
	28650 (0.02)	86, 88→92
	29450 (0.01)	87→92; 85→89*
	29500 (0.02)	86, 88→92*
31400 (62.0)	30100 (0.09)	86→99
	31000 (0.83)	84→89; 85→91 (vm) π→π*
40300 (49.3)	*etc.*	π→π*

[a] See Fig. 3. Numbers in parentheses are the molar absorptivity (10^{-3} M^{-1} cm^{-1}) followed by the bandwidth in cm^{-1}. [b] Values calculated by the ZINDO method (Reimers/Hush code) as previously described.[20–28] Numbers in parentheses are calculated oscillator strengths. All bands with oscillator strengths of at least 0.01 are reported. Predicted bands above 31000 cm^{-1} are less accurate and are not included. Energies are rounded to the nearest 50 cm^{-1}. [c] See text and Table 1 for the nature of these transitions, and supplementary material for pictures of the orbitals concerned. All the transitions are MLCT except where indicated otherwise. (vm) signifies an extensive mixture, due to configuration interaction, of many transitions of which only the major ones are cited. Cautionary note: because of the presence of so many overlapping bands, the 1:1 correspondence shown here between experimental and predicted bands, should be considered illustrative rather than definitive.

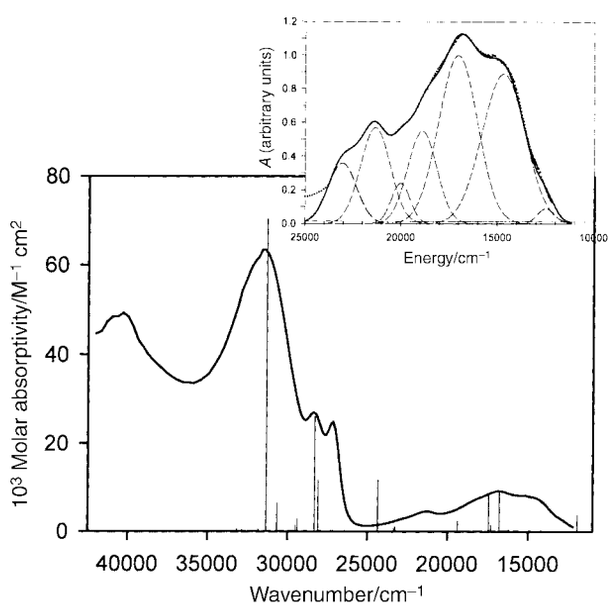

Fig. 3 (a) Electronic absorption spectrum of Ru(ddbbbpy)Cl_2 in CH_2Cl_2. The vertical bars are the ZINDO/S calculated energies with oscillator strengths scaled to the maximum of the visible absorption (see Experimental section). (inset) Curve fitting analysis of d→π* MLCT manifold. Experimental data indicated by a dotted line and a bold solid line represents the sum of the Gaussians (lines) used in analysis. See text.

during oxidation to generate $[Ru^{III}(ddbbbpy)Cl_2]^+$. The change in the electronic spectrum that results during the controlled-potential oxidation is essentially identical to that shown previously for the dimethyl analog (Fig. 4 of ref. 19). It is shown as supporting information (Fig. S2). The species exhibits no absorption in the near-infrared region. The neutral parent complex $Ru^{II}(ddbbbpy)Cl_2$ is diamagnetic based on its sharp NMR spectrum and silent EPR signal at room and low temperature. The low temperature (77 K) EPR spectrum of $[Ru(ddbbbpy)Cl_2]^+$ produced coulometrically by electrolysis at 0.72 V *vs.* NHE was recorded in frozen methylene chloride–

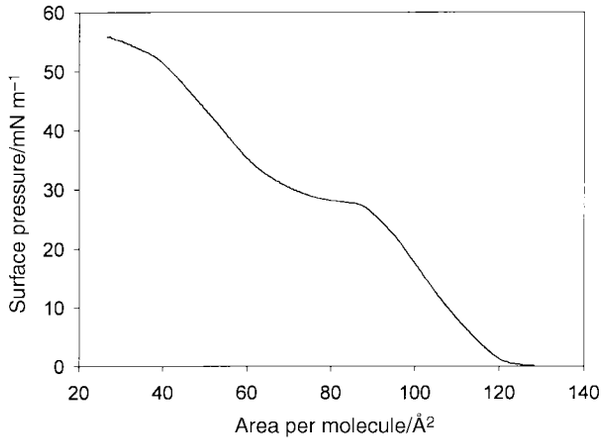

Fig. 4 Surface pressure–area (π–*A*) isotherm for the title complex at 20 °C on a pure water surface recorded at a linear compression speed of 20 mm min^{-1}.

methyltetrahydrofuran. The oxidation product was previously ascribed (for the R = Me species[19]) to formation of a Ru(III) species and this is confirmed in the current work by an EPR spectrum typical for a rhombohedrally distorted Ru(III) complex with *g* values of 2.73, 2.20 and 1.82 for (arbitrarily labeled) g_x, g_y and g_z respectively.[38] A relatively large rhombic distortion is manifest by the difference in the three *g* values, *i.e.*, the non-degenerate components of $g_\perp$, consistent for a planar C_2 symmetrical complex and the non-degeneracy of the two equivalent sets of coordinating nitrogen atoms of the ddbbbpy chelate.[38]

Langmuir films

***π–A* Isotherms.** The *π–A* isotherms of Ru(ddbbbpy)Cl_2 spread from $CHCl_3$ solutions onto pure water at 20 °C were recorded at several barrier compression rates. The mean area occupied by a molecule at monomolecular coverage is determined to be 115 ± 3 $Å^2$ and does not vary with compression speed. The isotherm (Fig. 4) indicates that the complex begins to pack at an area per molecule of ≈126 $Å^2$. The isotherms then become steep with a limiting molecular area of ≈91 $Å^2$ and a collapse pressure of 28 mN m^{-1} consistent with data for other ruthenium–bipyridine surfactant derivatives.[16] By using crystallographic data[14e,39–41] or the ZINDO optimized structure, the largest cross sectional area for Ru(ddbbbpy)Cl_2 is approximately 150 $Å^2$. From these data, the tilt angle for the molecule lying on the subphase surface can be approximated at ≈30°. Yamada and co-workers[11b] determined tilt angles of 38° for various $Ru(bpy)_3^{2+}$ surfactants bearing hexadecyl and octadecyl alkyl chains albeit their data pertain to multilayer films on a solid substrate. The molecular orientation and tilt angles were attributed to weak surface interactions of the hydrophobic head groups with the solid substrates.

Interestingly, isotherms recorded at slow linear barrier-compression-speeds (0.5–3.0 mm min^{-1}) indicate that the monolayer film appears to collapse at 44 mN m^{-1} with a corresponding area per molecule (APM) of ≈60 $Å^2$ and an estimated tilt angle of 66°. The APM is very small for a molecule as large as Ru(ddbbbpy)Cl_2 although small APM values and thus large tilt angles have been reported for phthalocyanines and related complexes.[42,43] Isotherms recorded at barrier speeds of 5–50 mm min^{-1} more clearly show monolayer collapse consistent with a large complex with a large cross-sectional area.[6a] Monolayer films are readily transferred from the trough to solid substrates indicative of the stability of the film. For example, electrostatic intermolecular and intramolecular interactions increase as the film is compressed, *i.e.*, intermolecular π–π interactions of the aromatic portion of the ligands and π–CH interactions resulting from the alkyl chains and the conjugated portion of the ligand.[44] Strong π–π interactions may

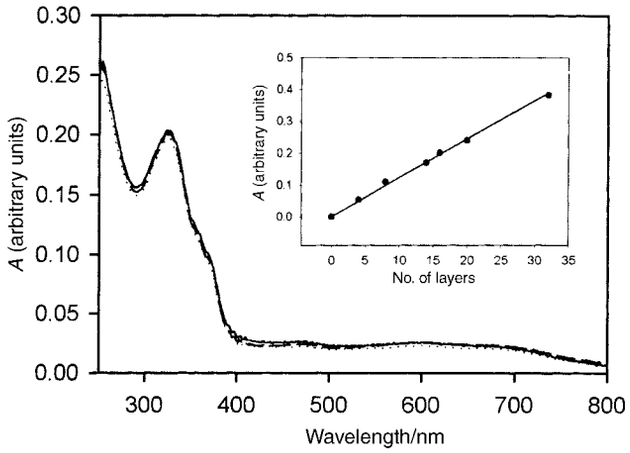

Fig. 5 Electronic absorption spectra of Ru(ddbbbpy)Cl_2 recorded as LB film 20 layers thick (5 cycles of Y-type transfer) at a deposition pressure of 17 mN m^{-1}. Films transferred from monolayers formed at compression speeds of 1 (solid), 5 (– – – –), and 20 (·····) mm min^{-1} (in order of decreasing intensity). The correlation of absorbance (λ_{max} = 324) *vs.* number of layers transferred is shown inset.

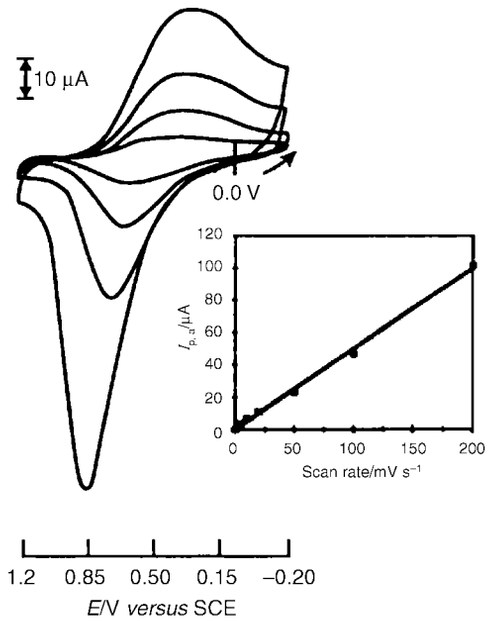

Fig. 6 Cyclic voltammetry of 20 layers of Ru(ddbbbpy)Cl_2 deposited on ITO electrodes at a deposition pressure of 17 mN m^{-1} in 0.2 M KCl aqueous solution. Inset is corrected anodic peak current *versus* scan rates of the potential sweep.

lead to aggregation of the film,[5] but repeated compression–decompression cycles of the monolayer show hysteresis in the isotherm. Reproducible compression–decompression cycling also demonstrate that the monolayer film does not polymerize during compression.[5d]

Electronic absorption spectra. Absorption spectra of the Langmuir–Blodgett films of Ru(ddbbbpy)Cl_2 are shown in Fig. 5. The films were transferred at a surface pressure of 17 mN m^{-1} and 5 cycles of Y-type transfer resulting in 20 layers. The most intense absorption lies at 30900 cm^{-1} in the electronic spectra of these LB film layers. The absorption is slightly greater for samples fabricated at slower compression speeds (inset of Fig. 5) inferring better film formation and transferability presumably due to better film organization. Although the transfer ratios of the monolayer to substrate were all ostensibly unity, an increase in absorption may be due to a more efficiently closed packed film formed at slow speeds thus giving more sample per area than films transferred at faster speeds.

Several ligand π–π* bands observed in the solution spectra disappear in the spectra of the LB films and the absorption maxima at 31400 cm^{-1} is shifted down 500 cm^{-1}. This may indicate weak intermolecular π–π interactions between the aromatic portion of the chelates in the layered films; a broadening of the ligand-based π–π* bands into a single broad manifold supports this hypothesis.[44] A consistent amount of material is transferred to the substrate after each deposition cycle is complete as noted by the linear plot of absorption *vs.* number of layers (inset, Fig. 5). Polarized spectra of the LB films were recorded at angles of 0° and 60° to the normal of the substrate surface. An increase in σ-polarized absorption and a decrease in π-polarized absorption is observed in the spectrum recorded at 60° relative to the 0° spectrum supporting that the film is canted by ≈30° on the substrate's surface, and more generally, arguing for organization of the film.

The electronic spectrum of the monolayer recorded on a pure water subphase (a mirror is placed under the surface to reflect back the incident beam) is similar to the spectra of the LB multilayer films transferred to and recorded on a substrate; no discernible shift in the λ_{max} at 324 nm was observed. Additionally, absorption of the monolayer increases with an increase in the surface pressures of the monolayer (from 5 mN m^{-1} to 30 mN m^{-1}) as would be expected as the APM decreases and thus the film surface density increases.

Electrochemistry. Examination of the electrochemical properties of the films of Ru(ddbbbpy)Cl_2 is essential toward understanding the potential uses for such complexes as molecular electronic devices. The electrochemical properties of thin films of Ru(ddbbbpy)Cl_2 were studied by using cyclic voltammetry on films comprised of 20 monolayers (5 Y-type transfers) transferred on to hydrophobic indium doped tin oxide (ITO) electrodes in aqueous solution with 0.2 M KCl as supporting electrolyte. The conductivity of the films was confirmed through observation of quasi-reversible cyclic voltammograms. Fig. 6 shows the voltammograms for Ru(ddbbbpy)Cl_2 recorded at scan rates of 20, 50, 100 and 200 mV s^{-1}. An average $E_{\frac{1}{2}}$ = 0.70 V *vs.* NHE (0.46 *vs.* SCE) for the surface waves was measured as compared to 0.63 *vs.* NHE in solution. The solution $E_{\frac{1}{2}}$ value was recorded in a non-polar media with a platinum working electrode while the surface potential was recorded in a dilute aqueous KCl solution and these differences likely account for differences in the two oxidation potentials. At higher scan rates, the peak-to-peak separation increases, accompanied by an increase in $i_{p,a}/i_{p,c}$ and a broadening of the reduction wave. The increase in peak-to-peak separation may be due to poor contact between Ru(ddbbbpy)Cl_2 and the electrode surface perhaps stemming from interferences with the long alkyl chains or distortion in the aromatic backbone of the chelate, the relatively large resistance of the ITO electrode, or an orientation of the complex on the slide that results in kinetically inefficient electron-transfer.[45] As described in the Experimental section, the ITO slides are hydrophobic, thus the first monolayer of Ru(ddbbbpy)Cl_2 is transferred to the slide with the alkyl tails in contact with the electrode surface with the redox active metal center situated away from the ITO surface. Accordingly, the lipophilic alkyl groups create an additional barrier for electron transfer as manifested by an increase in the broadness of the waves at increasing scan rates.

The voltammograms are quasi-reversible in that the ratio $i_{pa}/i_{p,c}$ is greater than unity. The slope of the graph of the anodic peak current *versus* scan rate (inset in Fig. 6) is 4.8×10^{-4} A s V^{-1} with a correlation coefficient of 0.999. Non-linear behavior at scan rates in the range of 20–500 mV s^{-1} was not observed regardless of the large resistivity of the ITO electrode and an increased barrier for electron transfer due to the insulating alkyl chains. Deviations from linearity at higher scan rates illustrated through broadening of the cathodic peak current have also been attributed to the kinetics of the flow of counter anions,

needed to maintain charge balance, in and out of the absorbed film. For example, at fast scan rates, anion diffusion through the film is slower than the CV time scale: anions can readily diffuse through the films but once the film is oxidized, outward anionic diffusion is slow. The Cl^- counter ions apparently migrate through the film which indicates that monolayers of $Ru(ddbbbpy)Cl_2$, are self-assembled in a diffuse manner due to van der Waals interactions of the long alkyl chains.[43]

From the peak current of the voltammograms and the area of the electrode surface, an approximation of the concentration of $Ru(ddbbbpy)Cl_2$ on the electrode surface can be determined from eqn. (1), where A is the surface area of the electrode, $i_{p,a}$ is

$$i_{p,a} = n^2F^2vA\Gamma/4RT \quad (1)$$

derived from eqn. (2), Γ is the concentration (mol m^{-2}) of the absorbed substance, n = no. of electrons transferred during oxidation, v = the potential scan rate, $R = 4.184$ J mol^{-1} K^{-1} and T = the cell temperature. From eqn. (1), an estimate of the surface concentration of $\Gamma = 1.75$ mol m^{-2} is derived leading to a value of 95 Å^2 per molecule consistent with the APM derived from the LB studies described earlier.[46,47]

Conclusions

The title complex is readily prepared in high yield from $RuCl_2(Me_2SO)_4$. The complex has a rich charge transfer spectrum in the visible region attributed to $d_\pi \rightarrow p_{\pi^*}$ transitions to the three lower lying unoccupied orbitals of the tetra-imine ligand. An unusual d_δ back-donation mechanism is noted. The complex is soluble in weakly polar organic solvents which facilitates its study by using Langmuir–Blodgett methods. The electronic absorption spectra of thin films of $Ru(ddbbbpy)Cl_2$ on a solid substrate lose some of the optical features observed in the solution spectrum and more closely resemble solid-state spectra. Thin films of $Ru(ddbbbpy)Cl_2$ are conductive as demonstrated by the quasi-reversible cyclic voltammograms of the films formed on ITO electrodes. Further modifications of the complex will be necessary in order to utilize $Ru(ddbbbpy)Cl_2$ for application purposes.

Experimental

Preparation of dichloro(6,6′-bis(*N*-dodecylbenzimidazol-2-yl)-2,2′-bipyridine)ruthenium(II)

A solution of $RuCl_2(Me_2SO)_4$ (96 mg, 0.20 mmol) and 6,6′-bis(*N*-dodecylbenzimidazole)-2,2′-bipyridine (150 mg, 0.21 mmol) in degassed toluene or methylene chloride (25 mL) was refluxed for 2 hours. The solution volume was reduced *in vacuo* followed by addition of acetone (10 mL). The resulting solution was poured into diethyl ether (200 mL) and the solution cooled in a refrigerator for 2 hours to complete precipitation. The dark purple powdery product was then collected by filtration, washed several times with diethyl ether and dried: yield 130 mg, 73%. ^{1}H NMR (500 MHz, $(CD_3)_2SO$): δ 8.59 (2H, d, $J = 7.6$, H_1), 8.50 (4H, d, $J = 8.2$, H_3 and H_a), 8.03 (2H, d, $J = 8.1$, H_d), 7.86 (2H, t, $J = 7.9$, H_2), 7.70 (4H, m, $J = 8.3$, H_c and H_b), 0.84 (6H, t, J = 12.8, $C_{11}H_{22}CH_3$). Shifts from δ 3.37 to 0.84 integrate for 50H. Anal. Calc. for $C_{48}H_{64}Cl_2N_6Ru\cdot H_2O$: C, 63.00; H, 7.27; N, 9.18. Found: C, 63.10; H, 7.25; N, 9.19%.

Physical measurements

Electronic spectra were recorded with a CARY 2400 UV-vis-NIR spectrophotometer for solutions and with a HP 8354 diode array processor for LB films. Electrochemical measurements were obtained with a PINE instruments RDE3 potentiostat. The working electrode was either glassy carbon or a platinum button electrode and the auxiliary electrode was a platinum plate. The ferrocenium/ferrocene couple was used as an internal calibrant (0.45 V *versus* AgCl/Ag or 0.67 *vs*. NHE in CH_2Cl_2).[48] For the LB film work, a normal three-electrode cell was used with the ITO slide serving as the working electrode and Pt wire and SCE used as counter and reference electrodes, respectively. Solutions were degassed by Ar bubbling prior to all electrochemical measurements. An optically thin cell was used to collect spectro-electrochemical data with the CARY 2400 spectrophotometer and the PINE electrochemical potentiostat. Spectra were taken at or near the oxidation potential of the title complex. Given the thickness of the cell (0.25 mm), five minutes was typically sufficient to complete the bulk electrolysis at a selected potential. Spectra were recorded at a selected potential step until no further change in the spectrum was observed. Electron paramagnetic resonance spectra were obtained with a Varian E4 spectrophotometer and were calibrated against diphenylpicrylhydrazyl (DPPH). ^{1}H NMR were measured with a 300 MHz Brüker instrument or a 500 MHz JEOL spectrometer with tetramethylsilane used as an internal standard.

Isotherm measurements and formation of LB films

Pressure–area isotherms of $Ru(dddbpy)Cl_2$ were recorded on a KSV (Stratford, CT) 3000 Langmuir–Blodgett trough modified to operate double barriers. Purified water (resistivity of 18 MΩ cm) was used in all the LB experiments. Langmuir monolayers were formed by spreading 80 μL of a 1.4×10^{-4} M chloroform solution of $Ru(dddbpy)Cl_2$ onto an aqueous subphase. After allowing for solvent evaporation and molecular reorganization, about 5 minutes, the monolayer was compressed at speeds from 0.5 mm min^{-1} to 100 mm $min.^{-1}$ Surface pressure was measured with a platinum Wilhelmy plate suspended from a KSV microbalance.

Glass microscope slides used for recording absorption spectra were first cleaned by using the RCA cleaning procedure and then dried under nitrogen.[49] Octadecyltrichlorosilane, OTS, was self-assembled onto the substrates to make them hydrophobic. The clean slides were immersed into a 2% solution of OTS in hexadecane for 2 hours, and dried under nitrogen. Hydrophobic ITO slides were used as provided.

For the UV-Vis and electrochemical studies, Langmuir monolayers were compressed to a pressure of 17 mN m^{-1} and bilayers were transferred onto hydrophobic substrates at speeds of 15 mm min^{-1} on the upstroke and downstroke. During film transfer, the Langmuir monolayer was held at a constant pressure and the films were formed by continuous deposition at the air/water interface. Multilayers were deposited onto substrates with transfer ratios of approximately unity.

Computational studies

Geometry optimizations were carried out by the INDO/1 method and used a developmental version[50] of ZINDO running on a Silicon Graphics Computer and with Ru, $\beta(4d) = -20$ eV.[34] These optimized files were then used as input for a further round of geometry optimization using Hyperchem 5.1 (Hypercube, Florida, v 5.1) running on a Pentium III 600 MHz Intel computer. The electronic spectra, orbital energies and mixing coefficients were calculated with ZINDO/S using a code kindly supplied by Reimers and Hush.[51] This utilized the ruthenium INDO/S parameter set obtained by Krogh-Jespersen *et al.*[52] Interaction factors were $k_{p\sigma} = 1$ and 1.267 and $k_{p\pi} = 1$ and 0.585 for ZINDO/1 and ZINDO/S respectively. The configuration interaction calculation, with ZINDO/S, used the 400 lowest energy singly excited configurations exciting from orbitals 68 to 88 into 89 to 108. Increasing the number of configurations had little effect on the predicted transition energies. Oscillator strengths of electronic transitions were calculated in the dipole length approximation including the one-center sp and pd atomic terms. Fig. 3 shows the predicted energies as bars. The predicted oscillator strengths were scaled to the experimental data by fitting the maximum intensity absorption in the visible

region. We are scaling oscillator strengths to molar absorptivity so that a direct match cannot be expected due to undoubted variations in bandwidth. Nevertheless a general fit can be anticipated.

The molecular orbitals shown in Fig. 1, 2 were generated by the Hyperchem 5.1 programme. The orbital energies and percent mixing derived for the frontier orbitals using this programme were extremely close to those predicted by the Reimers/Hush code. The mixing coefficients were calculated using the MOMIX program ver. 4 written by by S. I. Gorelsky and A. B. P. Lever. This programme, which can be used to process output from a variety of codes, is available from the authors.

Acknowledgements

A. B. P. L. and R. A. M thank the Natural Sciences and Engineering Research Council (Ottawa) for financial support. M. F. R. gratefully acknowledges the support of Purdue University Calumet and York University. M.-a. H. acknowledges financial support from the Ministry of Education, Science, Sports and Culture for a Grant-in-Aid for Scientific Research on Priority Areas of "Metal-assembled Complexes" and "Chemistry of Conjugated System". We are pleased to acknowledge Candace T. Seip and Daniel R. Talham of the University of Florida, Gainesville, for discussions and for technical assistance with the Langmuir–Blodgett procedures.

References

1 For some general references see: (*a*) N. Sutin and C. Creutz, *Pure Appl. Chem.*, 1980, **52**, 2717; (*b*) R. A. Krause, *Struct. Bonding* (*Berlin*), 1987, **67**, 1; (*c*) A. Juris, V. Balzani, F. Barigelletti, S. Campagna, P. Belser and A. Von Zelewsky, *Coord. Chem. Rev.*, 1988, **84**, 85; (*d*) V. Balzani, L. De Cola, L. Prodi and F. Scandola, *Pure Appl. Chem.*, 1990, **62**, 1457; (*e*) V. Balzani and F. Scandola, *Supramolecular Photochemistry*, Ellis Horwood, Chichester, 1991; (*f*) S. Van Walleddael and D. O. Rillema, *Coord. Chem. Rev.*, 1991, **111**, 297; (*g*) N. Fletcher, R. F. Keene, H. Viebrock and A. von Zelewsky, *Inorg. Chem.*, 1997, **36**, 1113; (*h*) B. Meir, T. Werner, I. Klimant and O. S. Wolfbeis, *Sens. Actuators, B*, 1995, **29**, 240; (*i*) I. Sasaki, M. Imberdis, M. A. Gaudemer and B. Drahi, *New J. Chem.*, 1994, **18**, 759.

2 E. A. Seddon and K. R. Seddon, *The Chemistry of Ruthenium*, Elsevier, New York, 1984.

3 For some references on redox active sensors see: (*a*) K. Maness, H. Masui, M. R. Wightman and R. W. Murray, *J. Am. Chem. Soc.*, 1997, **119**, 3987; (*b*) A. Wu, J.-K. Lee and M. F. Rubner, *Mater. Res. Soc. Symp. Proc.*, 1998, **488**, 63; (*c*) K. Tennakone, G. R. R. A. Kumura, I. R. M. Kottegoda and K. G. U. Wijayantha, *J. Phys. D: Appl. Phys.*, 1998, **31**, 1492; (*d*) A. Dernzier, P. Jardon, A. Martre, J.-C. Moutet, C. Santano, V. Balzini, A. Credi, F. Paolucci and S. Roffia, *New. J. Chem.*, 1998, **22**, 33; (*e*) H.-T. Zhang, S. G. Yan, P. Subramanian, L. M. Skeens-Jones, C. Stern and J. T. Hupp, *J. Electroanal. Chem.*, 1996, **414**, 23; (*f*) T. R. I. Cataldi, D. Centonze and A. Guerrieri, *Anal. Chem.*, 1995, **67**, 101.

4 For some references on photoinduced sensors see: (*a*) S. Yamada, M. Kawazu and T. Matsuo, *J. Chem. Phys.*, 1994, **98**, 3573; (*b*) H. Sakaguchi, L. A. Gomez-Jahn, M. Pritchard, T. L. Penner and D. G. Whitten, *J. Chem. Phys.*, 1993, **97**, 1474; (*c*) I. K. Lednev, E. V. Os'kina and M. V. Alfimov, *Vys. Energ.*, 1990, **24**, 461; (*d*) S. Fanni, T. E. Keyes, S. Campagna and J. G. Vos, *Inorg. Chem.*, 1998, **37**, 5933.

5 (*a*) G. G. Roberts (Editor) *Langmuir Blodgett Films*, Plenum, New York, 1990; (*b*) J.-M. Lehn, *Angew. Chem., Int. Ed. Engl.*, 1990, **29**, 1304; (*c*) B. Tieke, *Adv. Mater.*, 1990, **2**, 222; (*d*) A. Ulman, *An Introduction to Ultrathin Organic Films*, Academic, New York, 1991.

6 (*a*) K. M. De Armond and G. A. Fried, *Prog. Inorg. Chem.*, 1997, **44**, 97; (*b*) J.-K. Lee, D. S. Yoo, E. S. Handy and M. F. Rubner, *Appl. Phys. Lett.*, 1996, **69**, 1686; (*c*) A. Wu, J. Lee and M. F. Rubner, *Thin Solid Films*, 1998, **327**, 663; (*d*) A. M. Bond, G. B. Deacon, J. Howitt, D. R. Macfarlane, L. Spicci and G. Wolfbauer, *J. Electrochem. Soc.*, 1999, **146**, 648; (*e*) J. Luo and S. S. Isied, *Langmuir*, 1998, **14**, 3602; (*f*) H. O. Finlea and M. S. Ravenscroft, *Isr. J. Chem.*, 1997, **37**, 179; (*g*) A. Deronzier and M. Essakalli, *J. Chem. Soc., Chem. Commun.*, 1990, 242; (*h*) A. Alagna, A. Capobianchi, G. Pennesi, T. Prosperi and Rossi, *J. Phys. IV*, 1997, **7**, 1261; (*i*) T. R. I. Cataldi and G. E. De Bendetto, *J. Electroanal. Chem.*, 1998, **458**, 149; (*j*) T. R. I. Cataldi, G. E. De Bendetto and C. Campa, *J. Electroanal. Chem.*, 1997, **437**, 93.

7 K. Aoki, K. Kumazawa and Y. Ohsawa, *Thin Solid Films*, 1992, **213**, 295.

8 (*a*) A. H. De Armond, O. Dvorak, K. M. De Armond and H. P. Adams, *Thin Solid Films*, 1993, **232**, 115; (*b*) K. M. De Armond and H. Samha, *Langmuir*, 1994, **10**, 343.

9 (*a*) X. Zhang and A. J. Bard, *J. Am. Chem. Soc.*, 1989, **111**, 8098; (*b*) C.-W. Lee and A. J. Bard, *Chem. Phys. Lett.*, 1990, **170**, 57; (*c*) C. J. Miller and A. J. Bard, *Anal. Chem.*, 1991, **63**, 1707.

10 (*a*) H. Daifuku, K. Aoki, K. Tokuda and H. Matsuda, *J. Electroanal. Chem.*, 1985, **183**, 1; (*b*) H. Daifuku, I. Yoshimura, I. Hirata, K. Aoki, K. Tokuda and H. Matsuda, *J. Electroanal. Chem.*, 1986, **199**, 47; (*c*) T. Murakata, T. Miyashita and M. Matsuda, *Macromolecules*, 1989, **22**, 2706; (*d*) H. Sakaguchi, T. Nagamura, T. L. Penner and D. G. Whitten, *Thin Solid Films*, 1994, **244**, 947.

11 (*a*) T. Nagamura, H. Sakaguchi and T. Matsuo, *Thin Solid Films*, 1992, **210/211**, 162; (*b*) S. Yamada, T. Nakano and T. Matsuo, *Thin Solid Films*, 1994, **245**, 196.

12 H. A. Samha, T. J. Martinez, M. K. De Armond, F. O. Garces and R. J. Watts, *Inorg. Chem.*, 1993, **32**, 2583.

13 H. Samha and K. M. De Armond, *Coord. Chem. Rev.*, 1991, **111**, 73.

14 (*a*) R. A. Krause, *Inorg. Chim. Acta*, 1977, **22**, 209; (*b*) B. Durham, S. R. Wilson, D. J. Hodges and T. J. Meyer, *J. Am. Chem. Soc.*, 1980, **102**, 600; (*c*) J. L. Walsh and B. Durham, *Inorg. Chem.*, 1981, **21**, 329; (*d*) P. Bonneson, J. L. Walsh, W. T. Pennington, A. W. Cordes and B. Durham, *Inorg. Chem.*, 1983, **22**, 1761; (*e*) B. J. Coe and T. J. Meyer, *Inorg. Chem.*, 1993, **32**, 4012; (*f*) M. A. Masood, B. P. Sullivan and D. J. Hodges, *Inorg. Chem.*, 1994, **33**, 5360; (*g*) B. J. Coe, T. J. Meyer and P. S. White, *Inorg. Chem.*, 1995, **34**, 593.

15 A. W. Snow and W. R. Barger, in *Phthalocyanines: Properties and Applications*, ed. C. C. Leznoff and A. B. P. Lever, VCH, New York, 1989, vol. 1, p. 341.

16 (*a*) P. K. Chan, D. A. Isabirye and C. K. Poon, *Inorg. Chem.*, 1975, **14**, 2579; (*b*) D. D. Walker and H. Taube, *Inorg. Chem.*, 1981, **20**, 2828; (*c*) R. S. de Silva and E. Tfouni, *Inorg. Chem.*, 1992, **31**, 3313; (*d*) B. Dietrich, P. Viout and J.-M. Lehn, *Macrocyclic Chemistry*, VCH, New York, 1993; (*e*) J. R. Thornbuck and G. Wilkinson, *J. Chem. Soc., Dalton Trans.*, 1978, 110.

17 (*a*) E. V. Does and L. J. Wilson, *Inorg. Chem.*, 1978, **17**, 2660; (*b*) M. Haga, *Inorg. Chim. Acta*, 1980, **45**, L183; (*c*) M. Haga, T. Matsumura-Inoue and S. Yamabe, *Inorg. Chem.*, 1981, **26**, 4148; (*d*) M. Haga, *Inorg. Chim. Acta*, 1983, **75**, 29; (*e*) C. Long and J. G. Vos, *Inorg. Chim. Acta*, 1984, **89**, 125; (*f*) D. P. Rillema, R. Sahai, P. Matthews, A. K. Edwards, R. J. Shaver and L. Morgan, *Inorg. Chem.*, 1990, **29**, 167; (*g*) V. Goulle and R. P. Thummel, *Inorg. Chem.*, 1990, **29**, 1767; (*h*) M. Haga, T. Ano, K. Kano and S. Yamabe, *Inorg. Chem.*, 1991, **30**, 3843; (*i*) A. A. Batista, E. A. Polato, S. L. Queiroz and O. R. Nascimento, *Inorg. Chim. Acta*, 1995, **230**, 111; (*j*) K. B. Reddy, M. O. P. Cho, J. F. Wishart, T. J. Emge and S. S. Isied, *Inorg. Chem.*, 1996, **35**, 7241.

18 H. Monjushiro, K. Harada, M. Nakaura, N. Kato, M. Haga, M. F. Ryan and A. B. P. Lever, *Mol. Cryst. Liq. Cryst. Sci. Technol., Sect. A*, 1997, **294**, 15.

19 K. Mizushima, M. Nakaura, S.-B. Park, H. Nishiyama, H. Monjushiro, K. Harada and M. Haga, *Inorg. Chim. Acta*, 1996, **261**, 175.

20 (*a*) W. P. Anderson, T. C. Cundari, R. S. Drago and M. C. Zerner, *Inorg. Chem.*, 1989, **29**, 1; (*b*) W. P. Anderson, T. C. Cundari and M. C. Zerner, *Int. J. Quantum Chem.*, 1991, **39**, 31; (*c*) W. P. Anderson, W. D. Edwards and M. C. Zerner, *Inorg. Chem.*, 1986, **25**, 2728.

21 (*a*) M. C. Zerner, *Int. J. Quantum Chem.*, 1989, **35**, 567; (*b*) W. D. Edwards and M. C. Zerner, *Theor. Chim. Acta*, 1987, **72**, 347.

22 C. Martin and M. C. Zerner, in *Inorganic Electronic Structure and Spectroscopy*, ed. E. I. Solomon and A. B. P. Lever, Wiley and Sons, New York, 1999, vol. 1, p. 555.

23 A. D. Bacon and M. C. Zerner, *Theor. Chim. Acta*, 1979, **53**, 21.

24 M. C. Zerner, *Metal-Ligand Interactions*, Kluwer Academic Publishers, Dordrecht 1996, pp. 493.

25 M. C. Zerner, G. H. Loew, R. F. Kirchner and U. T. Mueller-Westerhoff, *J. Am. Chem. Soc.*, 1980, **102**, 589.

26 J. C. Culberson, P. Knappe, N. Rösch and M. C. Zerner, *Theor. Chim. Acta*, 1987, **71**, 21.

27 J. Ridley, J. and M. C. Zerner, *Theor. Chim. Acta*, 1973, **32**, 111.

28 J. Ridley, J. and M. C. Zerner, *Theor. Chim. Acta*, 1976, **42**, 223.
29 (*a*) R. A. Metcalfe and A. B. P. Lever, *Inorg. Chem.*, 1997, **36**, 4762; (*b*) R. A. Metcalfe, L. C. G. Vasconcellos, H. Mirza, D. W. Franco and A. B. P. Lever, *J. Chem. Soc.*, *Dalton Trans.*, 1999, 2653.
30 A. Broo and P. Lincoln, *Inorg. Chem.*, 1997, **36**, 2544.
31 (*a*) A. M. McDonagh, I. R. Whittall, M. G. Humphrey, D. C. R. Hockless, B. W. Skelton and A. H. White, *J. Organomet. Chem.*, 1996, **523**, 33; (*b*) A. M. McDonagh, I. R. Whittall, M. G. Humphrey, B. W. Skelton and A. H. White, *J. Organomet. Chem.*, 1996, **519**, 229.
32 (*a*) Y. G. Shin, B. S. Brunschwig, C. Creutz and N. Sutin, *J. Phys. Chem.*, 1996, **100**, 8157; (*b*) Y. G. Shin, B. S. Brunschwig, C. Creutz, M. D. Newton and N. Sutin, *J. Phys. Chem.*, 1996, **100**, 1104; (*c*) Y. G. Shin, B. S. Brunschwig, C. Creutz and N. Sutin, *J. Am. Chem. Soc.*, 1995, **117**, 8668.
33 O. V. Sizova, N. V. Ivanova, A. Y. Ershov, A. B. Nikolskii and I. V. Rogachevskii, *Zh. Obshch. Khim.*, 1997, **67**, 1409; O. V. Sizova, N. V. Ivanova and A. B. Nikolskii, *Zh. Obshch. Khim.*, 1997, **67**, 26; O. V. Sizova, A. I. Panin, N. V. Ivanova and V. I. Baranovskii, *J. Struct. Chem.*, 1997, **38**, 366.
34 S. I. Gorelsky, E. S. Dodsworth, A. A. Vlcek and A. B. P. Lever, *Coord. Chem. Rev.*, 1998, **174**, 469.
35 I. P. Evans, A. Spencer and G. Wilkinson, *J. Chem. Soc.*, *Dalton. Trans.*, 1973, 205.
36 (*a*) M. B. Gillian and J. E. Fergusson, *Aust. J. Chem.*, 1971, **24**, 441; (*b*) J. D. Birchall, T. D. O'Donoghue and J. R. Wood, *Inorg. Chim. Acta*, 1979, **37**, L461.
37 A. B. P. Lever, *Inorganic Electronic Spectroscopy*, Elsevier, Amsterdam, 2nd edn., 1984.
38 (*a*) N. Bag, G. K. Lahiri and A. J. Chakravorty, *Chem. Soc.*, *Dalton Trans.*, 1990, 1557; (*b*) P. H. Rieger, *Coord. Chem. Rev.*, 1994, **135/136**, 203.
39 M. Biner, H.-B. Bürgi, A. Ludi and C. Röhr. *J. Am. Chem. Soc.*, 1992, **114**, 5197.
40 J. March, *Advanced Organic Chemistry*, Wiley Interscience, New York, 4th edn., 1992.
41 D. R. Lide (Editor) *CRC Handbook of Chemistry and Physics*, CRC Press, Boca Raton, FL, 1991.
42 T. Richardson, G. G. Roberts, R. Barghout, R. G. Compton and D. J. Riley, *Electroanalysis* (*N. Y.*), 1985, **89**, 5698.
43 Y. Fu, M. Forman, C. C. Leznoff and A. B. P. Lever, *J. Phys. Chem.*, 1994, **98**, 8985.
44 M. Haga, N. Kato, H. Monjushiro, K. Wang and D. Md. Hossain, *Supramol. Sci.*, 1998, **5**, 337.
45 Y. Fu, J. Ouyang and A. B. P. Lever, *Phys. Chem.*, 1993, **97**, 13753.
46 Because eqn. (1) requires accurate $i_{p,a}$ values, to avoid errors due to imprecise baseline measurements,[47] anodic peak currents ($i_{p,a}$) were calculated from the uncorrected cathodic peak current $i_{p,c}$ and the current at the inversion potential $(i_\lambda)_0$ as given in eqn. (2). Derived $i_{p,a}$ values in Fig. 6 (inset) were calculated from eqn. (2). The current at

$$i_{p,a} / i_{p,c} = (i_{p,a})_0 / i_{p,c} + [0.485 ((i_\lambda)_0 / i_{p,c})] + 0.086 \quad (2)$$

inversion potential $(i_\lambda)_0$ is defined as the difference in $i_{p,c}$ (measured from the current axis) and the current at the switching potential, E_λ. [47] The value $(i_{p,a})_0$ is the peak current measured from the current axis whereas $i_{p,a}$ is the current measured from the baseline of the voltammogram.

Values for the ratios of $i_{p,a}/i_{p,c}$ were typically 2.1 ± 0.3 within the scan rates range of 5–200 mV s^{-1} and from these ratios, values of $i_{p,a}$ used in the graph in Fig. 6 (inset) were determined.
47 (*a*) A. J. Bard and L. R. Faulkner, *Electrochemical Methods*, Wiley, New York, 1980, ch. 12; (*b*) C. M. A. Brett and A. M. Olivera-Brett, *Electrochemistry: Principles*, *Methods*, *and Applications*, Oxford Press, New York, 1993, ch. 9.
48 A. B. P. Lever, E. R. Milaeva and G. Speier, in *Phthalocyanines: Properties and Applications*, ed. C. C. Leznoff and A. B. P. Lever, Wiley-VCH, New York, 1993, vol. 3, p. 1.
49 W. Kern, *J. Electrochem. Soc.*, 1990, **137**, 1887.
50 M. C. Zerner, ZINDO program, version 98.1, Quantum Theory Project, University of Florida, Gainesville, FL, 1998.
51 J. Zeng, N. S. Hush and J. R. Reimers *J. Phys. Chem.*, 1996, **100**, 19292.
52 K. Krogh-Jespersen, J. D. Westbrook, J. A. Potenza and H. J. Schugar, *J. Am. Chem. Soc.*, 1987, **109**, 7025.